# Preparation of Au/CeO$_2$ Exhibiting Strong Surface Plasmon Resonance Effective for Selective or Chemoselective Oxidation of Alcohols to Aldehydes or Ketones in Aqueous Suspensions under Irradiation by Green Light

Atsuhiro Tanaka, Keiji Hashimoto, and Hiroshi Kominami*

Department of Applied Chemistry, Faculty of Science and Engineering, Kinki University, Kowakae, Higashiosaka, Osaka 577-8502, Japan

ABSTRACT: Au/CeO$_2$ samples with various Au contents were prepared by the multistep (MS) photodeposition method. Their properties including Au particle size, particle dispersion, and photoabsorption were investigated and compared with properties of samples prepared by using the single-step (SS) photodeposition method. The MS- and SS-Au/CeO$_2$ samples were used for selective oxidation of benzyl alcohols to corresponding benzaldehydes in aqueous suspensions under irradiation by visible light from a green LED, and the correlations between reaction rates and physical properties of the MS- and SS-Au/CeO$_2$ samples were investigated. Difference in the two photodeposition methods was reflected in the average size and number of Au nanoparticles, for example, 92 nm and 1.3×10^{12} (g-Au/CeO$_2$)$^{-1}$ for MS photodeposition and 59 nm and 4.8×10^{12} (g-Au/CeO$_2$)$^{-1}$ for SS photodeposition in the case of 1.0 wt % Au samples. Fixation of larger Au particles resulted in strong photoabsorption of the MS-Au/CeO$_2$ samples at around 550 nm due to the surface plasmon resonance, and the Kubelka−Munk function of the photoabsorption linearly increased with increase in Au content up to 2.0 wt %, in contrast to the photoabsorption of SS-Au/CeO$_2$ samples, which was weak and was saturated even at around 0.5 wt %. Due to the strong photoabsorption, the MS-Au/CeO$_2$ samples exhibited reaction rates approximately twice larger than those of SS-Au/CeO$_2$ samples with the same Au contents, and apparent quantum efficiency of MS-Au/CeO$_2$ reached 4.9% at 0.4 mW cm^{-2}. Linear correlations were observed between reaction rates (r) and surface area of Au nanoparticles (S) in both MS- and SS-Au/CeO$_2$ samples, though the two slopes of r versus S plots were different, suggesting that oxidation of benzyl alcohol occurred on the Au surface and that S was one of the important factors controlling the reaction rate. Photocatalytic oxidation of benzyl alcohol having an amino group revealed that the Au/CeO$_2$ photocatalyst exhibited high chemoselectivity toward the hydroxyl group of alcohol, i.e, the Au/CeO$_2$ photocatalyst almost quantitatively converted aminobenzyl alcohol to aminobenzaldehyde with 99% yield.
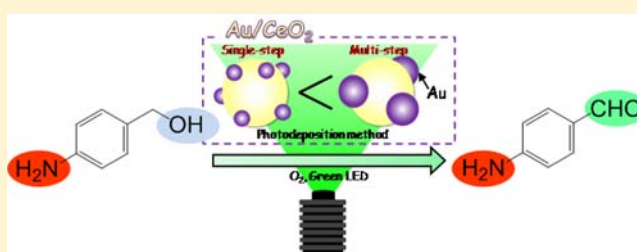
1. INTRODUCTION

Selective oxidation of aromatic alcohols to corresponding carbonyl compounds such as aldehydes and ketones without overoxidation to carboxylic acids and carbon dioxide remains a challenging task. Carbonyl compounds are widely used as intermediates for many fragrances, drugs, and vitamins. Selective oxidations to these compounds are carried out using stoichiometric oxidizing agents such as KMnO$_4$, MnO$_2$, CrO$_3$, and Br$_2$. However, these oxidations also give reduced residues of oxidizing agents. Since these reduced residues should be removed from the reaction mixtures and adequately recovered to prevent their diffusion in the environment, oxidations by stoichiometric oxidizing agents are costly methods and should be replaced with more environmentally friendly methods. Heterogeneous and homogeneous catalytic oxidation of alcohols to aldehydes or ketones with oxygen (O$_2$) molecules has been proposed as the most plausible method.[1] Only water (H$_2$O) is formed as the byproduct in these reactions, if the reactions ideally occur.

Oxidation by semiconductor photocatalysts such as titanium-(IV) oxide and tungsten(VI) oxide has attracted much attention and has been applied for purification of water and air[2] because holes and active oxygen species have strong oxidation power. However, selective (or partial) oxidation of organic compounds using semiconductor photocatalysts has been difficult due to the strong oxidation power. Since photocatalytic selective (or partial) oxidation occurs at room temperature under atmospheric pressure using O$_2$ molecules, the oxidation is still attractive for organic synthesis. Recently, several research groups have reported selective oxidation of aromatic compounds to carbonyl compounds using a TiO$_2$ photocatalyst.[3] Palmisano and co-workers[3c−g] demonstrated selective oxidation of benzyl alcohols to corresponding carbonyl compounds by O$_2$ in an aqueous solution by band gap excitation of rutile-type TiO$_2$ under UV irradiation. It is known

that UV light accounts for only about 5% of total solar energy, whereas visible light accounts for about 50%. Therefore, development of visible-light-responding photocatalysts is an important topic for chemical syntheses using solar energy in future. Many efforts have been devoted to synthesis of photocatalysts that respond to visible light, and various types of photocatalysts for mineralization of organic compounds have been reported.[4] However, to the best of our knowledge, there are no reports on selective oxidation of organic compounds using these visible-light-responding semiconductor photocatalysts. Different from these photocatalysts, selective oxidation of benzyl alcohol to benzaldehyde under irradiation by blue light from light-emitting diodes was reported by Higashimoto et al.[5] In their reaction system, benzyl alcohol was adsorbed on the surface of TiO_2 and electrons were transferred from the surface complex to TiO_2 under irradiation by visible light, resulting in formation of benzaldehyde and reduction of O_2 molecules.

Unique optical properties of metallic nanoparticles have been applied in many different fields including biochemistry, sensing science, and catalysis. Nanoparticles of metals such as copper (Cu), silver (Ag), and gold (Au) show strong photoabsorption of visible light due to surface plasmon resonance (SPR). However, there are limited reports on application of SPR-induced photoabsorption to chemical reactions, i.e., oxidation of organic substrates,[6d,e,7a,b] selective oxidation of aromatic alcohol to a carbonyl compound,[6c,7d] hydrogen formation from alcohols[6f,7e] and selective reduction of organic compounds.[6g] We examined mineralization of organic acid in aqueous suspensions of Au nanoparticles loaded on various metal oxides (Au/MOx) under visible light irradiation and found that Au loaded on cerium(IV) oxide (Au/CeO_2) was the most efficient photocatalyst among plasmonic Au/MOx photocatalysts.[7a,b] We also succeeded in shifting SPR to a longer length in copper (Cu)-Au/CeO_2 and mineralization of organic acids in an aqueous suspension of Cu-Au/CeO_2 even under irradiation by visible light of $\lambda = 700$ nm.[7c] In our previous communication,[7d] we briefly reported almost quantitative oxidation of benzyl alcohols to benzaldehydes in aqueous suspensions of Au/CeO_2 under irradiation by green light from an LED. By using the multistep (MS) photodeposition method[7c,e] in which addition of metal sources and photodeposition of the metals on semiconductor particles were repeated several times to obtain a desired metal loading, we succeeded in preparation of Au/CeO_2 exhibiting SPR absorption stronger than that of Au/CeO_2 prepared by using a single-step (SS) photodeposition method. In this paper, we report (1) characterization of Au/CeO_2 samples prepared by MS and SS photodeposition methods, (2) correlation between properties and photocatalytic activities of Au/CeO_2 in benzaldehyde formation, and (3) chemoselective oxidation of aminobenzyl alcohols to aminobenzaldehydes in aqueous suspensions of MS-Au/CeO_2 under irradiation by green light from an LED.

2. EXPERIMENTAL SECTION

2.1. Preparation of Au/CeO_2. Commercial highly pure (>99.99%) and fine spherical CeO_2 particles having a cubic structure and an average diameter of 0.2 μm were supplied by Kojundo Chemical Laboratory. Loading of Au on CeO_2 was performed by a photodeposition method. Bare CeO_2 powder (198 mg) was suspended in water (10 cm^3) in a test tube, and the test tube was sealed with a rubber septum under argon (Ar). An aqueous solution of

tetrachloroauric acid ($HAuCl_4$) was injected into the sealed test tube and then photoirradiated at λ >300 nm by a 400-W high-pressure mercury arc (Eiko-sha, Osaka, Japan) under Ar with magnetic stirring in a water bath continuously kept at 298 K. The Au source was reduced by photogenerated electrons in the conduction band of CeO_2, and Au metal was deposited on CeO_2 particles, resulting in the formation of Au/CeO_2. Analysis of the liquid phase after each photodeposition revealed that the Au source had been almost completely (>99.9%) deposited as Au on the CeO_2 particles. The resultant powder was washed repeatedly with distilled water and then dried at 310 K overnight under air. This photodeposition of Au was repeated several times to obtain an Au/CeO_2 sample having a desired Au content. This photodeposition method is called the MS photodeposition method and, hereafter, a sample prepared by the MS photodeposition method is designated as MS-Au(X)/CeO_2, where X means total Au content. The amount of Au loaded per a single deposition in MS photodeposition was generally 0.5 wt %, and an MS-Au(1.0)/CeO_2 sample was prepared by performing the photodeposition two times. The MS photodeposition method can be used flexibly, e.g., an MS-Au(1.0)/CeO_2 sample can also be prepared by first 0.50 wt % Au loading followed by 0.10 wt % loading five times (1.0 = 0.50 + 0.10 × 5). General photodeposition method in which all of the $HAuCl_4$ solution containing the desired amount of Au was injected, defined here as the SS photodeposition method, was used for comparison with the MS photodeposition method, and a sample prepared by the SS photodeposition method is designated as SS-Au(X)/CeO_2. It was confirmed that the Au source was also almost completely (>99.9%) deposited as Au on the CeO_2 particles when the SS photodeposition method was used.

2.2. Characterization. Diffuse reflectance spectra were obtained with a UV−vis spectrometer (UV-2400, Shimadzu, Kyoto) equipped with a diffuse reflectance measurement unit (ISR-2000, Shimadzu). The morphology of Au/CeO_2 particles was observed under a JEOL JEM-3010 transmission electron microscope (TEM) operated at 300 kV in the Joint Research Center of Kinki University.

2.3. Oxidation of Aromatic Alcohols in an Aqueous Suspension of Au/CeO_2 under Irradiation of Visible Light. The dried Au/CeO_2 powder (50 mg) was suspended in distilled water (5 cm^3), bubbled with O_2, and sealed with a rubber septum. Aromatic alcohol was injected into the suspension and then irradiated with visible light of a green light-emitting diode (HDMS8G, Hayashi Watch Works, Tokyo, maximum energy at 530 nm, designated green LED hereafter). The light intensity was fixed as 1.7 mW cm^{-2} unless otherwise stated. Since an LED consumes less energy than a fluorescent lamp, LEDs would be preferably used as light sources of photochemical processes in industry because of their low energy consumption. The amount of carbon dioxide (CO_2) in the gas phase was measured using a Shimadzu GC-8A gas chromatograph equipped with a Porapak QS column. The amounts of aromatic alcohols and aldehydes in the liquid phase were determined with a Shimadzu GC-14B gas chromatograph equipped with a DB-1 capillary column (30 m, 0.25 mm). Toluene was used as an internal standard sample. The reaction solution (1 cm^3) was added to a diethyl ether/water mixture (2:1 v/v, 3 cm^3). After the mixture had been stirred for 10 min, aromatic alcohols and aldehydes in the ether phase were analyzed. The amounts of aromatic alcohols and aldehydes were determined from the ratios of the peak areas of aromatic alcohols and aldehydes to the peak area of toluene.

3. RESULTS AND DISCUSSION

3.1. Characterization of SS- and MS-Au(X)/CeO_2 Samples. Figure 1a and b shows TEM photographs of SS- and MS-Au(1.0)/CeO_2 samples, respectively. In both cases, fine Au nanoparticles were observed within relatively sharp distributions. The average particle sizes of SS- and MS-Au(1.0)/CeO_2 samples were determined to be 59 and 92 nm with standard deviations of 4.9 and 8.0 nm, respectively.

These results indicate that the size of Au nanoparticles loaded on CeO_2 is strongly affected by the type of
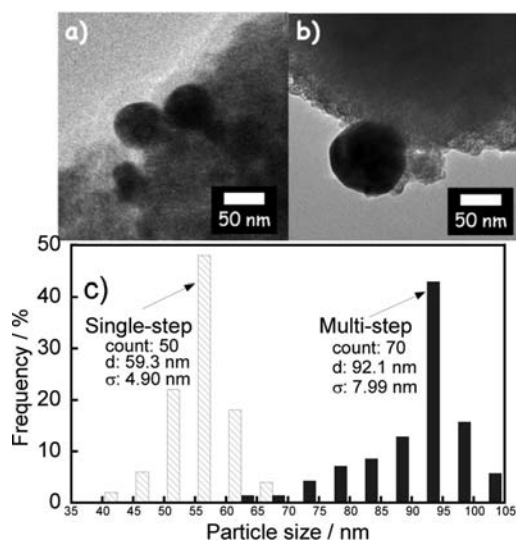
Figure 1. TEM images of (a) SS-Au(1.0)/CeO$_2$, (b) MS-Au(1.0)/CeO$_2$, and (c) size distributions of Au particles of SS- and MS-Au/CeO$_2$ samples.

photodeposition method and that there is a tendency for larger Au nanoparticles to be formed by the MS photodeposition method. Using SS and MS photodeposition methods, Au(X)/CeO$_2$ samples having various Au contents (X) were prepared.

Table 1 summarizes the average sizes of Au nanoparticles determined by TEM (D_{Au}) and number densities of Au nanoparticles (N_{Au}) calculated from D_{Au}, the density of Au metal (19.32 g cm^{-3}) and the amount of Au loaded on CeO$_2$ under the assumption that all of the Au nanoparticles were spherical. The D_{Au} values of Au nanoparticles in the SS- and MS-Au(X)/CeO$_2$ samples increased with increase in X, and the

Table 1. Various Properties of Au(X)/CeO$_2$ Samples Prepared by SS and MS Photodeposition Methods

method[a]	Au loading, wt %	D_{Au}[b] nm	N_{Au},[c] 10^{12} (g-Au/CeO$_2$)$^{-1}$	S_{Au},[d] 10^{-2} m^2 (g-Au/CeO$_2$)$^{-1}$
SS	0.1	19	14	1.6
	0.25	29	10	2.7
	0.5	39	8.3	4.0
	1.0	59	4.8	5.3
	1.5	64	5.6	7.2
	2.0	68	6.3	9.1
MS	1.0	92	1.3	3.4
	1.5	105	1.3	4.4
	2.0	115	1.3	5.4

[a]SS: single-step photodeposition method. MS: multistep photodeposition method. [b]D_{Au}: average size of Au nanoparticles calculated from the values of more than 50 particles observed by TEM. In the case of non-sphere particles such as ellipse, the largest diameter (the length of the major axis for ellipse) was regarded as the particle size. [c]N_{Au}: number density of Au nanoparticles in g-Au/CeO$_2$. This value was calculated from D_{Au}, density of metal (19.32 g cm^{-2}), and the amount of Au loaded on CeO$_2$ on the assumption that all of the particles were spheres. In the case of non-sphere particles such as ellipse particles, the assumption causes overestimation of the particle volume and underestimation of N_{Au}. [d]S_{Au}: external surface area of supported Au nanoparticles. This value was calculated from the average size of Au nanoparticles and N_{Au}. The values would be slightly overestimated because of particle–particle contact and particle-support contact.

D_{Au} values of MS-Au(X)/CeO$_2$ samples were always larger than those of SS-Au(X)/CeO$_2$ samples with the same X. The N_{Au} value of SS-Au(X)/CeO$_2$ samples decreased with increase in X and reached a minimum (4.8 × 10^{12} (g-Au/CeO$_2$)$^{-1}$) at X = 1.0 (Table 1). Further increase in X resulted in a slight increase in N_{Au}. These results suggest that balance of nucleation, growth and aggregation of Au particles changed depending on concentration of the Au source, which caused change of N_{Au} in the SS photodeposition method. It should be noted that the N_{Au} value of MS-Au(X)/CeO$_2$ samples was constant (1.3 × 10^{12} (g-Au/CeO$_2$)$^{-1}$), indicating that the Au source was deposited only on Au particles previously formed in the range from X = 1.0 to X = 2.0 in the MS photodeposition method and that neither new particle formation nor particle aggregation occurred.

In a previous study,[7e] it was found that the external surface area of Au (not the Au content) was an important factor controlling the photocatalytic activity of Au/CeO$_2$ in SPR-induced photocatalytic reaction.

Table 1 summarizes the external surface area (S_{Au}) calculated from D_{Au} and N_{Au}. The S_{Au} value of Au nanoparticles in the SS- and MS-Au(X)/CeO$_2$ samples increased with increasing X. The S_{Au} values of MS-Au(X)/CeO$_2$ samples were always smaller than those of SS-Au(X)/CeO$_2$ samples with the same X, corresponding to the larger D_{Au} values of MS-Au(X)/CeO$_2$ samples.

3.2. Observation of Growth of Au Nanoparticles Prepared by the MS Photodeposition Method. As stated above, the N_{Au} value of MS-Au(X)/CeO$_2$ samples was constant (1.3 × 10^{12} (g-Au/CeO$_2$)$^{-1}$) in the range of X = 1.0 to X = 2.0; however, there was a large gap between MS-Au(0.5)/CeO$_2$ (first 0.5 wt % Au deposition, identical to SS-Au(0.5)/CeO$_2$) and MS-Au(1.0)/CeO$_2$ prepared by repeating 0.5 wt % Au deposition (X = 1.0 = 0.5 × 2), i.e., the N_{Au} value of the former was 8.3 × 10^{12} (g-Au/CeO$_2$)$^{-1}$. This large decrease in N_{Au} suggests that the second added Au source decreased N_{Au}. In this experiment, the amount of Au added per photodeposition was reduced to 0.1 wt %, and the effect of a small addition of Au source on morphology and N_{Au} of MS-Au(X)/CeO$_2$ samples was examined. Figure 2a−d shows TEM photographs of thus-prepared MS-Au(X)/CeO$_2$ samples (X = 0.5 + 0.1 × n, n = 0, 2, 3, and 5). The particle size increased with repetition of photodeposition of 0.1 wt % Au, and contact between two nanoparticles was observed in the sample of X = 0.8 (n = 3) as shown in Figure 2c. This behavior is attributed to the decrease in N_{Au} in a series of MS-Au(X)/CeO$_2$ samples. Changes in N_{Au} values of the MS-Au(X)/CeO$_2$ samples are shown in Figure 2e. The N_{Au} values gradually decreased, indicating that contact between two Au nanoparticles occurred at any n except n = 0 depending on the size of each Au particle at n = 0 and the distance between two Au nanoparticles. Large decrease in the N_{Au} value was observed at around X = 0.7 and 0.8 (n = 2 and 3), and contact between Au particles occurred frequently at this range.

3.3. Photoabsorption Properties of SS- and MS-Au(X)/CeO$_2$ Samples. Figure 3 shows photoabsorption spectra of MS- and SS-Au(1.0)/CeO$_2$ samples. Strong photoabsorption was observed in both spectra at around 550 nm, and the strong photoabsorption was attributed to SPR of the supported Au nanoparticles.[6,7] It should be noted that MS-Au(1.0)/CeO$_2$ samples exhibited photoabsorption much stronger than that of SS-Au(1.0)/CeO$_2$ samples, although the amounts of Au (X) were the same. This result suggests that the intensity of
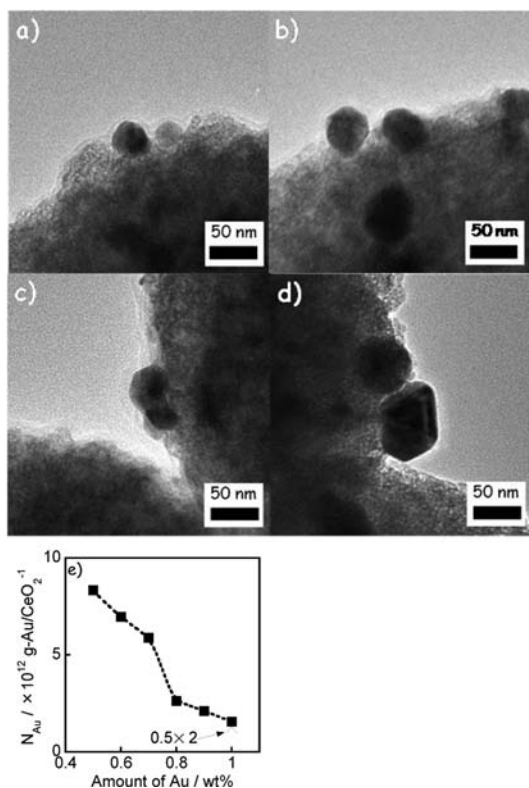
Figure 2. TEM images of MS-Au(X)/CeO$_2$ samples with various Au contents (X): (a) 0.5 wt %, (b) 0.7 wt % (= 0.5 + 0.1 × 2), (c) 0.8 wt % (= 0.5 + 0.1 × 3), and (d) 1.0 wt % (= 0.5 + 0.1 × 5). (e) Effect of X on N_{Au}.
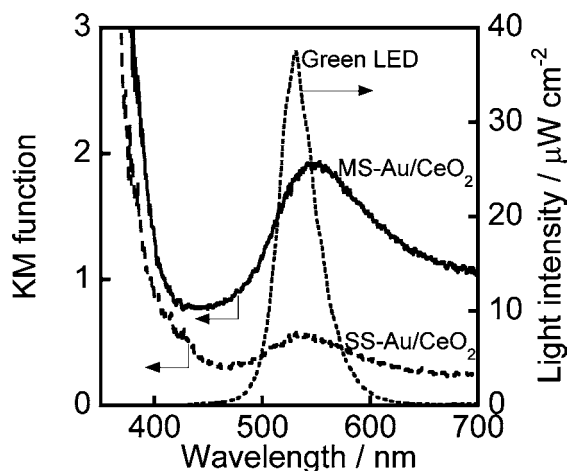
Figure 3. Absorption spectra of SS-Au(1.0)/CeO$_2$ (broken line) and MS-Au(1.0)/CeO$_2$ (solid line), and light intensity of visible light irradiated to reaction systems from a green LED (right axis).

photoabsorption due to SPR of Au was affected by the size of Au nanoparticles (Table 1). Similar results have been obtained in plasmonic Au/TiO$_2$ photocatalysts[7e] and unsupported Au nanoparticles.[8] In the latter case, Shimizu et al.[8] reported that such observed features coincide with the prediction of the Mie theory. As also shown in Figure 3, the photoabsorption property of Au/CeO$_2$ samples matched the wavelength of light emitted from a green LED.

Figure 4 shows the Kubelka−Munk function at 550 nm of SS- and MS-Au(X)/CeO$_2$ samples having various values of X. It
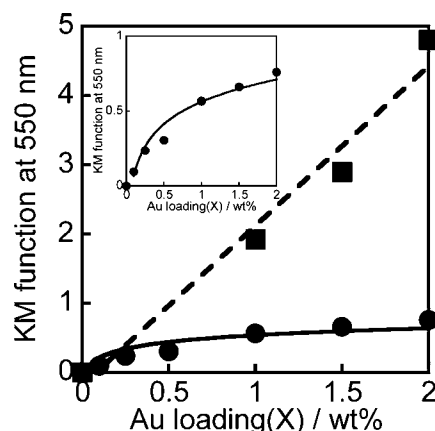
Figure 4. Kubelka−Munk function of photoabsorption at 550 nm of SS-Au(X)/CeO$_2$ (●) and MS-Au(X)/CeO$_2$ (■) having various Au contents (X).

is obvious that SS- and MS-Au(X)/CeO$_2$ samples showed different tendencies in the plots. The Kubelka−Munk function at 550 nm of MS-Au(X)/CeO$_2$ samples increased almost linearly until X = 2.0. The linear correlation between the Kubelka−Munk function and X in MS-Au(X)/CeO$_2$ samples indicates that Au nanoparticles fixed on CeO$_2$ effectively absorbed light corresponding to the amount (mass) of Au, as is observed for some chemical species in solution that absorb light corresponding to the concentration. On the other hand, the Kubelka−Munk function at 550 nm of SS-Au(X)/CeO$_2$ samples tended to be saturated (figure inserted inside). As shown in Table 1, the D_{Au} values of a series of SS-Au(X)/CeO$_2$ samples were smaller than 70 nm. The smaller particle size might be one of the reasons for the nonlinearity between SPR-absorption and X. From these results, we reach the conclusion that the MS photodeposition method is more effective for preparation of Au/CeO$_2$ exhibiting strong SPR.

3.4. Photocatalytic Oxidation of Benzyl Alcohol in Aqueous Suspensions. Figure 5 shows the time courses of photocatalytic oxidation of benzyl alcohol (33 μmol) in aqueous suspensions of SS- and MS-Au(1.0)/CeO$_2$ under irradiation by green light from an LED. We confirmed that benzyl alcohol was completely consumed after 20 h for SS-Au(1.0)/CeO$_2$ and after 15 h for MS-Au(1.0)/CeO$_2$, and no
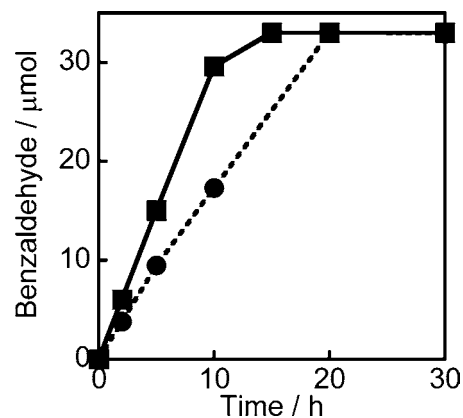
Figure 5. Time courses of benzaldehyde formation in photocatalytic oxidation of benzyl alcohol (33 μmol) in aqueous suspensions of SS-Au(1.0)/CeO$_2$ (●) and MS-Au(1.0)/CeO$_2$ (■) under irradiation by visible light from a green LED (1.7 mW cm^{-2}) in the presence of O$_2$.

CO_2 was detected in both cases during the photoirradiation. It should be noted that benzaldehyde was formed with quite high selectivity (>99%) at >99% conversion of benzyl alcohol, indicating that benzyl alcohol was almost quantitatively converted to benzaldehyde in the present photocatalytic reaction system under irradiation by green light from an LED. Since benzaldehyde increased linearly with photo-irradiation time, the rates of benzaldehyde formation for SS- and MS-Au(1.0)/CeO_2 samples were determined to be 1.9 and 3.0 μmol h^{-1}, respectively, i.e., MS-Au(1.0)/CeO_2 exhibited a rate of benzaldehyde formation ca. 1.6 times larger than that of SS-(1.0)Au/CeO_2. Intense SPR absorption of MS-Au/CeO_2 due to the larger Au particles is one of the main reasons for the larger activity for benzaldehyde production. Since MS-Au(1.0)/CeO_2 sample exhibited relatively strong photoabsorption even at around 600−700 nm, photocatalytic reaction of benzyl alcohol under irradiation with red light from a red LED (λ_{max} = 640 nm) was examined. After irradiation for 20 h, 5.2 μmol of benzyl alcohol was consumed and 5.1 μmol of benzaldehyde was formed, indicating that MS-Au(1.0)/CeO_2 sample worked for the oxidation of benzyl alcohol even under red light irradiation.

Photocatalytic oxidation of benzyl alcohol in aqueous suspensions of SS- and MS-Au(X)/CeO_2 samples having various values of X was examined using a green LED as the light source, and their rates of benzaldehyde formation were plotted against their S_{Au} (Figure 6). Linear correlations between
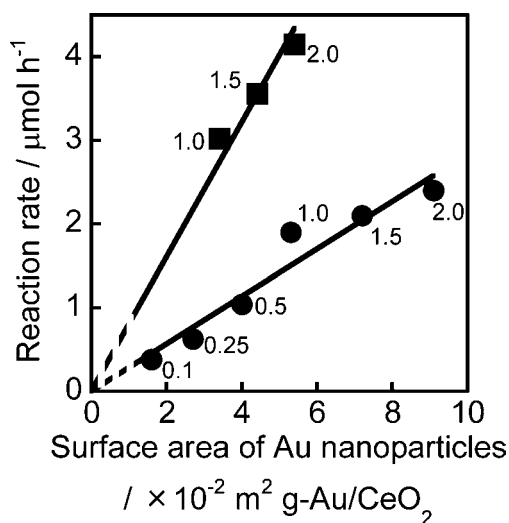

Figure 6. Effect of external surface area of Au nanoparticles of SS-Au(X)/CeO_2 (●) and MS-Au(X)/CeO_2 (■) on rate of benzaldehyde formation from aqueous solutions of benzyl alcohol in the presence of O_2 under irradiation by visible light from a green LED (1.7 mW cm^{-2}). Values in the figure are contents of Au (X).

the rate and S_{Au} were observed in both SS- and MS-Au(X)/CeO_2 samples. It should be noted that the slopes of the plots were different, and MS-Au(X)/CeO_2 samples showed a slope larger than that of SS-Au(X)/CeO_2 samples. These results suggest that the external surface area of Au loaded on CeO_2 and the intensity of photoabsorption due to SPR of Au nanoparticles are important factors controlling the photocatalytic activity of Au/CeO_2 regardless of the type of photodeposition method.

Oxidation of benzyl alcohol to benzaldehyde in aqueous suspensions of SS- and MS-Au(1.0)/CeO_2 samples was

examined under irradiation by light from a green LED with various light intensities (0.4−1.7 mW cm^{-2}) as shown in Figure 7a. Figure 7b shows the effect of light intensity on the rate of
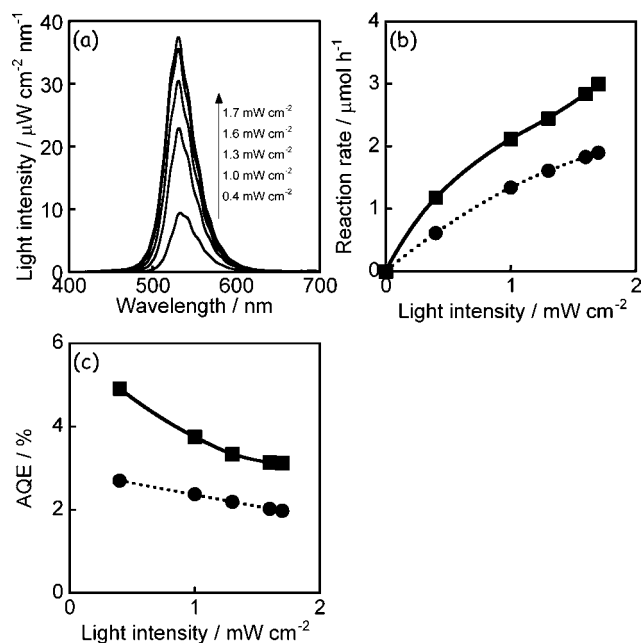
Figure 7. (a) Light intensity of visible light irradiated to reaction systems from a green LED and effect of light intensity on (b) the rate of benzaldehyde formation and (c) apparent quantum efficiency (AQE) in oxidation of benzyl alcohol to benzaldehyde in the presence of SS-Au(1.0)/CeO_2 (●) and MS-Au(1.0)/CeO_2 (■).

benzaldehyde formation. The rates increased with increase in light intensity in both cases, and the rates of MS-Au(1.0)/CeO_2 samples were always larger than those of SS-Au(1.0)/CeO_2. Apparent quantum efficiency (AQE) under irradiation by green light of an LED was determined to be 2.0% and 3.1%, respectively, at 1.7 mW cm^{-2}, i.e., MS-Au(1.0)/CeO_2 exhibited AQE ca. 1.8 times larger than that of SS-(1.0)Au/CeO_2. The effect of intensity of light on AQE is shown in Figure 7c, indicating that Au/CeO_2 samples worked effectively even under irradiation by weak green light from the LED. With decrease in the light intensity, AQE increased, and the value finally reached 4.9% and 2.7% for MS- and SS-Au(1.0)/CeO_2 samples, respectively, at 0.4 mW cm^{-2}, suggesting that Au/CeO_2 can be used in selective oxidation of benzyl alcohol by visible light from light sources such as an LED and the sun.

Photocatalytic oxidation of p-substituted benzyl alcohol in aqueous suspensions of SS- and MS-Au(1.0)/CeO_2 samples was investigated. Benzyl alcohol and its derivatives substituted by electron-donating groups (-NH_2, -OCH_3, and -CH_3) and electron-withdrawing groups (-Cl and -NO_2) were converted to the corresponding aldehydes with high rates of conversion and selectivity (>99%) on Au/CeO_2, while no other products were observed. The rate of p-substituted benzaldehyde formation in both Au/CeO_2 samples decreased in the order -NH_2 > -OCH_3 > -CH_3 > -H > -Cl > -NO_2, and this order indicates that the rate of p-substituted benzaldehyde formation is enhanced by electron-donating substituents and retarded by electron-with-drawing substituents. These rates showed a reasonably linear Hammett correlation as shown in Figure 8, and Hammett σ values of −1.77 (r^2 = 0.99) and −2.83 (r^2 = 0.99) were obtained for SS- and MS-Au(1.0)/CeO_2 samples, respectively.
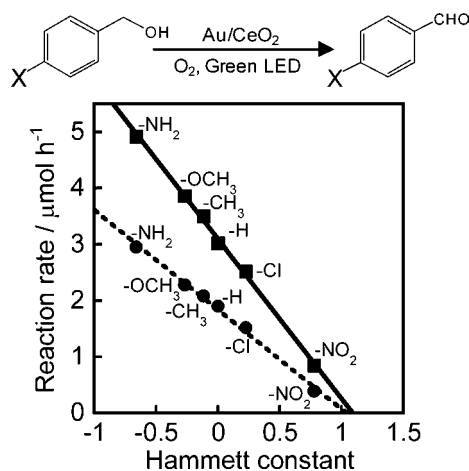
Figure 8. Hammett correlation study for photocatalytic oxidation of *p*-substituted benzyl alcohols in aqueous suspensions of SS-Au(1.0)/CeO$_2$ (●) and MS-Au(1.0)/CeO$_2$ (■) in the presence of O$_2$.

On the basis of consideration of the above results, a possible reaction mechanism for the photocatalytic oxidation of benzyl alcohol to corresponding aldehydes over Au/CeO$_2$ under visible light irradiation is shown in Scheme 1. This scheme is partially derived from the mechanism for electrochemical oxidation of benzyl alcohols to aldehydes.[9]

Scheme 1. Assumed Reaction Mechanism for the Photocatalytic Oxidation of Benzyl Alcohols over Au/CeO$_2$ under Visible Light Irradiation
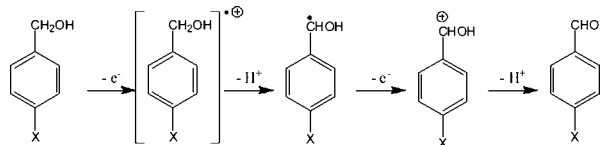

Under irradiation by visible light, incident photons are absorbed by Au particles through their SPR excitation, electrons may be injected from Au particles into the conduction band of CeO$_2$, and the resultant electron-deficient Au could oxidize organic compounds to be recovered to the original metallic state. The effective oxidation of electron-rich benzyl alcohol may be ascribed to smooth electron transfer from benzyl alcohol to electron-deficient Au. Since the present reaction is performed in the presence of O$_2$, electrons are trapped by O$_2$ and some active oxygen species would be formed. The candidates are ●O$_2^-$ radical (O$_2$ + e$^-$ → ●O$_2^-$) and/or H$_2$O$_2$ (O$_2$ + 2e$^-$ + 2H$^+$ → H$_2$O$_2$). Multielectron reduction of O$_2$ is preferred to one-electron reduction of O$_2$ in photocatalytic oxidations in the presence of metal co-catalysts. Very high selectivity of benzaldehyde in the present system suggests that active oxygen species were removed from the reaction system. Decomposition of H$_2$O$_2$ over Au nanoparticles was reported by Naya et al.[10]

3.5. Intramolecular and Intermolecular Chemoselective Oxidation of Aminobenzyl Alcohol. Chemoselective oxidation of an alcohol group of molecules that have an easily oxidized amino group is a challenge. We noticed that a high aldehyde yield (>99%) was obtained even in the presence of an amino group that is easily oxidized. Therefore, we examined photocatalytic oxidation of *p*-aminobenzyl alcohol (ABAL, 50

*μ*mol) in aqueous suspensions of MS-Au(1.0)/CeO$_2$ samples under irradiation by light from a green LED.

Figure 9 shows time courses of photocatalytic oxidation of ABAL. The amount of ABAL decreased linearly with
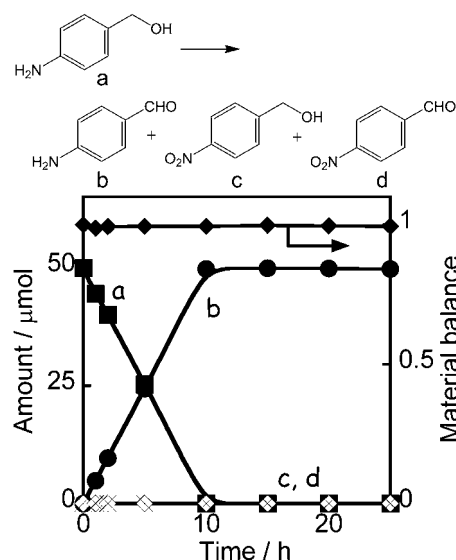

Figure 9. Time courses of the amounts of aminobenzyl alcohol (a), aminobenzaldehyde (b), nitrobenzyl alcohol (c), nitrobenzaldehyde (d), and material balance (◆, right axis) in aqueous suspensions of MS-Au(1.0)/CeO$_2$ under irradiation by green light from an LED (1.7 mW cm^{-2}) in the presence of O$_2$.

photoirradiation, while the amount of *p*-aminobenzaldehyde (ABAD) as the oxidation product of ABAL increased. ABAL was completely consumed after irradiation for 20 h, and no CO$_2$ was detected during the photoirradiation. Figure 9 clearly shows that ABAD was formed with quite high selectivity (>99%) at >99% conversion of ABAL with other oxidation products, i.e., *p*-nitrobenzyl alcohol and *p*-nitrobenzaldehyde, not being detected and that a high carbon balance (>99%) was always preserved. These results indicate that ABAL was chemoselectively and quantitatively converted to ABAD. The quite high chemoselectivity can be explained by the fact that ABAD formed was never converted to *p*-nitrobenzaldehyde with prolongation of photoirradiation.

After photocatalytic oxidation of *p*-aminobenzyl alcohol, MS-Au(1.0)/CeO$_2$ was recovered from the reaction mixture and was used for the same reaction. As shown in Figure 10, MS-Au(1.0)/CeO$_2$ worked as a reusable photocatalyst without loss of its activity and chemoselectivity at least 5 times.

The chemoselectivity of Au/CeO$_2$ for the hydroxyl group of alcohol was further investigated in intermolecular competitive reaction of benzyl alcohol and aniline (aminobenzene). In photocatalytic oxidation of an equimolar mixture of benzyl alcohol and aminobenzene in aqueous suspensions, we found that MS-Au(1.0)/CeO$_2$ gave only benzaldehyde as the product from benzyl alcohol after irradiation for 20 h, as shown in Figure 11. Oxidation of aminobenzene was observed after benzyl alcohol had been completely consumed. These results clearly demonstrated that the plasmonic Au/CeO$_2$ photocatalyst system under visible light in the presence of O$_2$ showed complete chemoselective oxidation toward the hydroxyl group of alcohol in the presence of an inter- and intramolecular amino group.
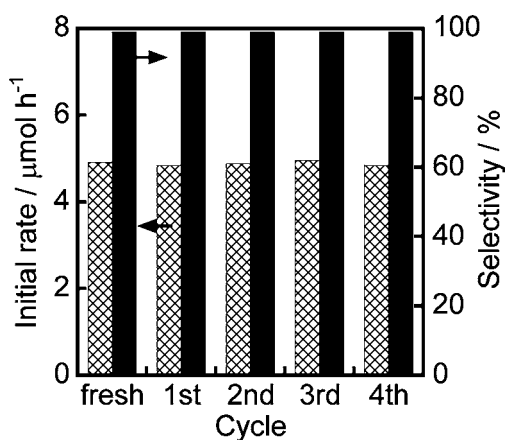
Figure 10. Chemoselective oxidation of *p*-aminobenzyl alcohol (50 μmol) to *p*-aminobenzaldehyde in an aqueous suspension of MS-Au(1.0)/CeO₂.
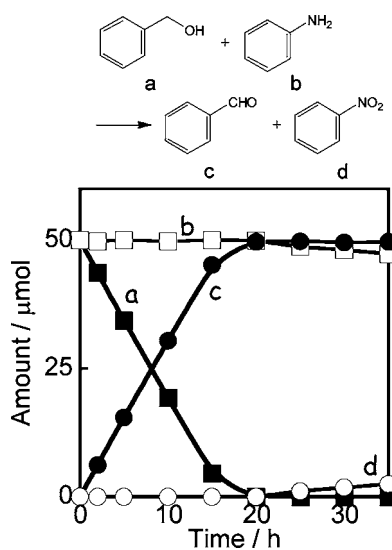
Figure 11. Intermolecular competitive oxidation of benzyl alcohol (a) and aniline (aminobenzene) (b) to benzaldehyde (c) and nitrobenzene (d), respectively, in aqueous suspensions of MS-Au(1.0)/CeO₂ under irradiation by green light from an LED (1.7 mW cm⁻²) in the presence of O₂.

3.6. Applicability of Au/CeO₂ for Selective Oxidation of Alcohols.

To expand the applicability of Au/CeO₂ for selective oxidation, photocatalytic oxidation of various alcohols other than benzyl alcohols in aqueous suspensions of SS- and MS-Au(1.0)/CeO₂ was examined under irradiation by green light from an LED. As shown in Table 2, SS- and MS-Au(1.0)/CeO₂ photocatalysts were also effective in oxidation of secondary aliphatic alcohol (2-pentanol), alicyclic alcohol (cyclohexanol), secondary aromatic alcohol (1-phenylethanol), and primary aromatic alcohol (2-phenylethanol) to corresponding aldehydes or ketones with quite high selectivities larger than 99%, indicating that the plasmonic Au/CeO₂ photocatalyst can be used for selective oxidation of various alcohol compounds. In all reaction systems, MS-Au(1.0)/CeO₂ exhibited activities higher than those of SS-Au(1.0)/CeO₂ as well as oxidation of benzyl alcohol.

Table 2. Oxidation of Various Alcohols in Aqueous Suspensions of MS- and SS-Au(1.0)/CeO₂ Samples under Irradiation by Green Light from an LED in the Presence of O₂[a]

Method	Substrate	Product	Time / h	Conv.[b] / %	Selectivity[b] / %
SS	OH (2-pentanol)	O (ketone)	25	39	>99
MS				45	>99
SS	OH (cyclohexanol)	O (cyclohexanone)	24	45	>99
MS				59	>99
SS	OH (1-phenylethanol)	O (acetophenone)	36	33	>99
MS				45	>99
SS	OH (2-phenylethanol)	CHO	56	13	>99
MS				17	>99

[a]Photocatalytic reactions: Au/CeO₂, 50 mg; water, 5 cm³; O₂, 1 atm; green LED, 1.7 mW cm⁻². [b]Determined by GC using the internal standard method.

4. CONCLUSIONS

Using the MS and SS photodeposition methods, Au/CeO₂ samples with various Au contents were prepared and their properties including Au particle size, particle dispersion and photoabsorption were investigated. Larger Au particles with smaller number were loaded on CeO₂ by the MS photodeposition method, whereas smaller Au particles with larger number were loaded by the SS photodeposition method. The MS-Au/CeO₂ samples exhibited very strong photoabsorption at around 550 nm due to surface plasmon resonance of Au nanoparticles, and the strong photoabsorption was attributed to the large Au particles. On the other hand, photoabsorption of the SS-Au/CeO₂ sample was weak, although Au content was the same. Different behaviors were also observed in effects of Au content on photoabsorption; the Kubelka–Munk function of the photoabsorption of MS-Au/CeO₂ samples linearly increased with increase in Au content up to 2.0 wt % with constant Au particle number, while the Kubelka–Munk function of photoabsorption of the SS-Au/CeO₂ sample was saturated even at around 0.5 wt %. Both the MS- and SS-Au/CeO₂ samples exhibited high selectivity in oxidation of benzyl alcohol to benzaldehyde in aqueous suspensions under visible light irradiation from a green LED, i.e., benzaldehyde was quantitatively formed in both cases. The formation rates by MS-Au/CeO₂ samples were ca. twice larger than those by SS-Au/CeO₂ samples, and apparent quantum efficiency of the MS-Au(1.0)/CeO₂ sample reached 4.9% at 0.4 mW cm⁻². The strong photoabsorption of MS-Au/CeO₂ samples was attributable to the large reaction rate. In both cases of MS- and SS-Au/CeO₂ samples, linear correlations were observed between the reaction rates and S_{Au}, although the slopes of the rate vs S_{Au} plots were different, indicating that the external surface area of Au nanoparticles rather than the Au content is one of the important factors controlling the reaction rate of Au/CeO₂ under visible light irradiation. Au/CeO₂ exhibited high chemoselectivity in both selective oxidation of aminobenzyl

alcohol to aminobenzaldehyde and intermolecular selective oxidation of benzyl alcohol to benzaldehyde in the presence of aniline. Aminobenzaldehyde was obtained almost quantitatively in the former case and only benzyl alcohol was converted to benzaldehyde with 99% yield in the latter case.

■ AUTHOR INFORMATION

Corresponding Author
hiro@apch.kindai.ac.jp

Notes
The authors declare no competing financial interest.

■ ACKNOWLEDGMENTS

■ REFERENCES

(1) (a) Yamaguchi, K.; Mori, K.; Mizugaki, T.; Ebitani, K.; Kaneda, K. *J. Am. Chem. Soc.* **2000**, *122*, 7144−7145. (b) Yamaguchi, K.; Mizuno, N. *Angew. Chem., Int. Ed.* **2002**, *41*, 4538−4541. (c) Tsunoyama, H.; Sakurai, H.; Negishi, Y.; Tsukuda, T. *J. Am. Chem. Soc.* **2005**, *127*, 9374−9375. (d) Abad, A.; Almela, C.; Corma, A.; Garcia, H. *Chem. Commun.* **2006**, 3178−3180. (e) Enache, D. I.; Edwards, J. K.; Landon, P.; Solsona-Espriu, B.; Carley, A. F.; Herzing, A. A.; Watanabe, M.; Kiely, C. J.; Knight, D. W.; Hutchings, G. J. *Science* **2006**, *311*, 362−365. (f) Lu, A. -H.; Li, W. -C.; Hou, Z.; Schuth, F. *Chem. Commun.* **2007**, 1038−1040. (g) Turner, M.; Golovko, V. B.; Vaughan, O. P. H.; Abdulkin, P.; Berenguer-Murcia, A.; Tikhov, M. S.; Johnson, B. F. G.; Lambert, R. M. *Nature* **2008**, *454*, 981−984. (h) Ng, Y. H.; Ikeda, S.; Harada, T.; Morita, Y.; Matsumura, M. *Chem. Commun.* **2008**, 3181−3183. (i) Dhakshinamoorthy, A.; Alvaro, M.; Garcia, H. *ACS Catal.* **2011**, *1*, 48−53. (j) Figiel, P. J.; Sibaouih, A.; Ahmad, J. U.; Nieger, M.; Raisanen, M. T.; Leskela, M.; Repo, T. *Adv. Synth. Catal.* **2009**, *351*, 2625−2632. (k) Zhang, N.; Fu, X.; Xu, Y. J. *J. Mater. Chem.* **2011**, *21*, 8152−8158. (l) Zhang, H.; Xie, Y.; Sun, Z.; Tao, R.; Huang, C.; Zhao, Y.; Liu, Z. *Langmuir* **2011**, *27*, 1152−1157.

(2) (a) Fox, M. A.; Dulay, M. T. *Chem. Rev.* **1993**, *93*, 341−357. (b) Hoffmann, M. R.; Martin, S. T.; Choi, W.; Bahnemann, D. W. *Chem. Rev.* **1995**, *95*, 69−96.

(3) (a) Pillai, U. R.; Sahle-Demessie, E. *J. Catal.* **2002**, *211*, 434−444. (b) Mohamed, O. S.; Gaber, A. E. M.; Abdel-Wahab, A. A. *J. Photochem. Photobiol. A* **2002**, *148*, 205−210. (c) Palmisano, G.; Yurdakal, S.; Augugliaro, V.; Loddo, V.; Palmisano, L. *Adv. Synth. Catal.* **2007**, *349*, 964−970. (d) Yurdakal, S.; Palmisano, G.; Loddo, V.; Augugliaro, V.; Palmisano, L. *J. Am. Chem. Soc.* **2008**, *130*, 1568−1569. (e) Augugliaro, V.; Caronna, T.; Loddo, V.; Marc, G.; Palmisano, G.; Palmisano, L.; Yurdakal, S. *Chem.—Eur. J.* **2008**, *14*, 4640−4646. (f) Yurdakal, S.; Palmisano, G.; Loddo, V.; Alagoz, O.; Augugliaro, V.; Palmisano, L. *Green Chem.* **2009**, *11*, 510−516. (g) Augugliaro, V.; Palmisano, L. *ChemSusChem* **2010**, *3*, 1135−1138. (h) Zhang, M.; Chen, C.; Ma, W.; Zhao, J. *Angew. Chem., Int. Ed.* **2008**, *47*, 9730−9733. (i) Zhang, M.; Wang, Q.; Chen, C.; Zang, L.; Ma, W.; Zhao, J. *Angew. Chem., Int. Ed.* **2009**, *48*, 6081−6084. (j) Wang, Q.; Zhang, M.; Chen, C.; Ma, W.; Zhao, J. *Angew. Chem., Int. Ed.* **2010**, *49*, 7976−7979.

(4) (a) Asahi, R.; Morikawa, T.; Ohwaki, T.; Aoki, K.; Taga, Y. *Science* **2001**, *293*, 269−271. (b) Ohno, T.; Akiyoshi, M.; Umebayashi, T.; Asai, K.; Mitsui, T.; Matsumura, M. *Appl. Catal., A* **2004**, *265*, 115−121. (c) Abe, R.; Takami, H.; Murakami, N.; Ohtani, B. *J. Am. Chem. Soc.* **2008**, *130*, 7780−7781. (d) Arai, T.; Horiguchi, M.; Yanagida, M.; Gunji, T.; Sugihara, H.; Sayama, K. *Chem. Commun.* **2008**, 5565−5567. (e) Irie, H.; Miura, S.; Kamiya, K.; Hashimoto, K. *Chem. Phys. Lett.* **2008**, *457*, 202−205. (f) Kisch, H.; Zang, L.; Lange, C.; Maier, W. F.; Antonius, C.; Meissner, D. *Angew. Chem., Int. Ed.* **1998**, *37*, 3034−3036. (g) Kitano, S.; Hashimoto, K.; Kominami, H. *Appl. Catal., B* **2011**, *101*, 206−211. (h) Tanaka, A.; Hashimoto, K.; Kominami, H. *Chem. Lett.* **2011**, *40*, 354−356.

(5) (a) Higashimoto, S.; Kitao, N.; Yoshida, N.; Sakura, T.; Azuma, M.; Ohue, H.; Sakata, Y. *J. Catal.* **2009**, *266*, 279−285. (b) Higashimoto, S.; Okada, K.; Morisugi, T.; Azuma, M.; Ohue, H.; Kim, T.-H.; Matsuoka, M.; Anpo, M. *Top. Catal.* **2010**, *53*, 578−583. (c) Higashimoto, S.; Suetsugu, N.; Azuma, M.; Ohue, H.; Sakata, Y. *J. Catal.* **2010**, *274*, 76−83. (d) Higashimoto, S.; Okada, K.; Azuma, M.; Ohue, H.; Terai, T.; Sakata, Y. *RSC Adv.* **2012**, *2*, 669−676.

(6) (a) Tian, Y.; Tatsuma, T. *J. Am. Chem. Soc.* **2005**, *127*, 7632−7637. (b) Furube, A.; Du, L.; Hara, K.; Katoh, R.; Tachiya, M. *J. Am. Chem. Soc.* **2007**, *129*, 14852−14853. (c) Naya, S.; Teranishi, M.; Isobe, T.; Tada, H. *Chem. Commun.* **2010**, *46*, 815−817. (d) Kowalska, E.; Abe, R.; Ohtani, B. *Chem. Commun.* **2009**, 241−243. (e) Kowalska, E.; Mahaney, O. O. P.; Abe, R.; Ohtani, B. *Phys. Chem. Chem. Phys.* **2010**, *12*, 2344−2355. (f) Yuzawa, H.; Yoshida, T.; Yoshida, H. *Appl. Catal., B* **2012**, *115*, 294−302. (g) Ke, X.; Sarina, S.; Zhao, J.; Zhang, X.; Chang, J.; Zhu, H. *Chem. Commun.* **2012**, *48*, 3509−3511.

(7) (a) Kominami, H.; Tanaka, A.; Hashimoto, K. *Chem. Commun.* **2010**, *46*, 1287−1289. (b) Kominami, H.; Tanaka, A.; Hashimoto, K. *Appl. Catal., A* **2011**, *397*, 121−126. (c) Tanaka, A.; Hashimoto, K.; Kominami, H. *ChemCatChem* **2011**, *3*, 1619−1623. (d) Tanaka, A.; Hashimoto, K.; Kominami, H. *Chem. Commun.* **2011**, *47*, 10446−10448. (e) Tanaka, A.; Sakaguchi, S.; Hashimoto, K.; Kominami, H. *Catal. Sci. Technol.* **2012**, *2*, 907−909.

(8) Shimizu, T.; Teranishi, T.; Hasegawa, S.; Miyake, M. *J. Phys. Chem. B* **2003**, *107*, 2719−2724.

(9) *Organic Electrochemistry*; Lund, H.; Hammerich, O., Eds.; Marcel Dekker: New York, 2001; p 611.

(10) Naya, S.; Teranishi, M.; Kimura, K.; Tada, H. *Chem. Commun* **2011**, *47*, 3230−3232.